Pair of Exceptional Points in a Microdisk Cavity under an Extremely Weak Deformation

Chang-Hwan Yi,[1,*] Julius Kullig,[1,2] and Jan Wiersig[1]

[1]*Institut für Theoretische Physik, Otto-von-Guericke-Universität Magdeburg, Postfach 4120, D-39016 Magdeburg, Germany*
[2]*Institut für Physik, Technische Universität Ilmenau, D-98693 Ilmenau, Germany*

One of the interesting features of open quantum and wave systems is the non-Hermitian degeneracy called an exceptional point, where not only energy levels but also the corresponding eigenstates coalesce. We demonstrate that such a degeneracy can appear in optical microdisk cavities by deforming the boundary extremely weakly. This surprising finding is explained by a semiclassical theory of dynamical tunneling. It is shown that the exceptional points come in nearly degenerated pairs, originating from the different symmetry classes of modes. A spatially local chirality of modes at the exceptional point is related to vortex structures of the Poynting vector.

Real physical systems are always open systems as they are never completely decoupled from their environment. Open quantum (wave) systems can exhibit exceptional points, in short EPs, in parameter space at which not only the energy levels (resonant frequencies) but also the corresponding eigenstates (modes) coalesce [1]. Because of its relation to other fascinating issues such as parity-time symmetry [2] or quantum phase transitions [3], EPs have attracted great attention recently. Intensive theoretical efforts have been devoted to study EPs in various fields such as hydrogen atoms [4], photonic lattices [5], and lasers [6] along with experimental verifications, e.g., in microwave [7] and optical [8] resonators.

There is another inevitable property of real physical systems in the context of dynamical system theory: non-integrability traced back to the impossibility of perfect symmetries in nature. This fundamental concern is studied in the research field of quantum chaos [9]. One of the remarkable results in this field is the dynamical tunneling through nonenergetic barriers in phase space [10]. Among several classifications of it [11], so-called "resonance-assisted tunneling" (RAT), inducing an enhanced coupling of eigenmodes due to nonlinear resonance chains [12] placed in between the modes, has been considered as very useful in describing near-integrable systems [13,14]. Various experiments have confirmed the importance of dynamical tunneling in, e.g., quantum dots [15], optical microcavities [16], microwave systems [17], and cold atoms [18].

Deformed optical microdisks are quasi-two-dimensional systems that serve as an outstanding example to study both the openness and the nonintegrability [19]. Up to now, EPs [20] and RAT [21–23] in microcavities have been investigated separately. In the present Letter, we combine these two aspects and reveal the explicit role of RAT in the formation of EPs in weakly deformed microdisks. Since the

deformation in this Letter is extremely weak and preserves a simple-connected smooth convex boundary, this perturbation is radically different from the ones reported in [24]. In addition, fruitful characteristics of the EP for applications, e.g., ultrasensitive sensing of particles [24,25], are addressed.

As a generic example, we consider the cavity

$$x^2 + y^2(1 + \varepsilon x^2/R^2) = R^2, \qquad (1)$$

where the deformation parameter ε is dimensionless. For $\varepsilon = 0$, the cavity is the integrable case of a circle of radius R. The corresponding ray dynamical phase space is foliated by invariant curves of constant angular momentum; see Fig. 1(a). For small ε, the system is near integrable with a prominent single $(t{:}r)$-resonance chain in phase space. In this regime, practically no chaotic layer and subisland structures around this main resonance chain can be seen.
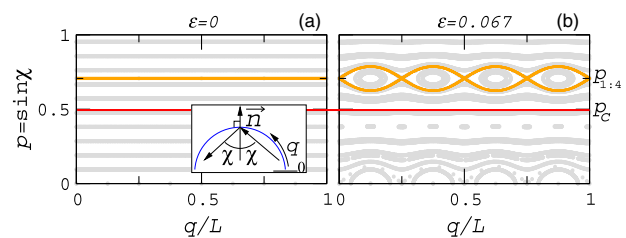
FIG. 1. Phase space of the ray dynamics (Poincaré surface of section) in the cavity (1); $q \in [0, L]$ is the arclength coordinate along the boundary with perimeter L and $p = \sin\chi \in [-1, 1]$ is the tangential component of the normalized momentum of the incident ray. Only the part with $p > 0$ is shown corresponding to counterclockwise propagating rays. Curves are generated by plotting a dot at (q, p) whenever a ray is reflected from the cavity's boundary. p_c marks the critical line for total internal reflection; $n = 2$. The resonance chain is shown by the thick curve around $p_{1:4}$ in (b).

Here, $t = 1$ and $r = 4$ are rotation and bouncing numbers of the central periodic ray at $p_{1:4} = 1/\sqrt{2}$; see Fig. 1(b). When the effective index of refraction is $n > \sqrt{2}$, the critical line $p_c = 1/n$ for total internal reflection is located under this resonance chain. Hereafter, we focus on this situation.

The optical modes are defined as (damped) time-harmonic solutions of Maxwell's equations with Sommerfeld's outgoing-wave condition and the transverse magnetic polarization condition across the cavity boundary. In this setup, the modes are expressed by the wave function $\psi(x, y) = E_z(x, y)$ where E_z is the z component of the electric field vector. Since the cavity in Eq. (1) has a mirror-reflection symmetry with respect to both x and y axes, the modes can be classified into even-even (EE), even-odd (EO), odd-even (OE), and odd-odd (OO) parities. We mainly deal with the EE parity. For the circular cavity, the mode pairs OO-EE and EO-OE are degenerated in their (complex-valued) dimensionless frequency kR, which can be obtained analytically by solving the equation [26]

$$S_m(kR; n) \equiv n \frac{J'_m}{J_m}(nkR) - \frac{H_m^{(1)'}}{H_m^{(1)}}(kR) = 0, \qquad (2)$$

where J, J', H, and H' are the Bessel function, the derivative of it, the Hankel function of first kind, and the derivative of it, respectively. Beside the angular mode number m there is a radial mode number l labeling the solutions of Eq. (2) for fixed m.

For a (1:4)-resonance chain the RAT occurs between the modes fulfilling the Fermi resonance condition [14,27] $(\Delta l, \Delta m) = (1, 4)$. The first step of our scheme is to determine for fixed (l, m) the refractive index $n = n_{\text{EP}}$ such that $\text{Re}(k_{l,m}R) = \text{Re}(k_{l+1,m-4}R)$ using Eq. (2). These degenerate points appear in Fig. 2 as peaks. Shown is the degree of degeneracy

$$\Delta^{-1} \equiv [\text{Re}(k_{l,m}R) - \text{Re}(k_{l+1,m-4}R)]^{-1}, \qquad (3)$$

as a function of n and m for several l. Experimentally, n cannot be varied over a wide range without changing the
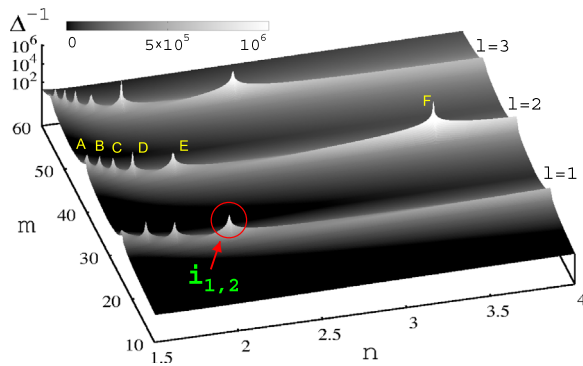
material. However, one can choose a material with n close to a peak in Fig. 2 and then fine-tune the effective index of refraction n by fabricating several samples with a different disk height. In the following, we consider the pair $(l, m) = (1, 22)$ and $(2, 18)$, which is labeled $i_{1,2}$ in Fig. 2.

The next step is to slightly deform the cavity by increasing ε. The frequencies are calculated using the boundary element method (BEM) [28]. For the sake of clear visibility, we use the shifted frequency $\kappa = \kappa_r + i\kappa_i \equiv n(k - \bar{k})R$ with mean frequency $\bar{k} = (k_{l,m} + k_{l+1,m-4})/2$. Figure 3 shows the branching of the real and imaginary parts of frequencies at an EP at $(n_{\text{EP}}, \varepsilon_{\text{EP}}) \approx (2.1051, 0.000\,434)$ on the path connecting the points $i_{1,2}$ and $f_{1,2}$. This EP is of second order; i.e., exactly two eigenvalues and eigenstates coalesce. Remarkably, the EP can be reached by varying ε alone and it occurs at an extremely weak deformation $\varepsilon < 10^{-3}$.

Now, we make the link between the observed EP and RAT more explicit. The $(t:r)$-resonance chain [see Fig. 1(b) for (1:4)] of the weakly deformed cavity can be approximated by the pendulum Hamiltonian [21,29],

$$\mathcal{H}(p) = -\frac{(p - p_{t:r})^2}{\sqrt{1 - p_{t:r}^2}} + 2\mathcal{V}_{t:r} \cos\left(r\frac{q}{L}2\pi + \phi_0\right), \qquad (4)$$
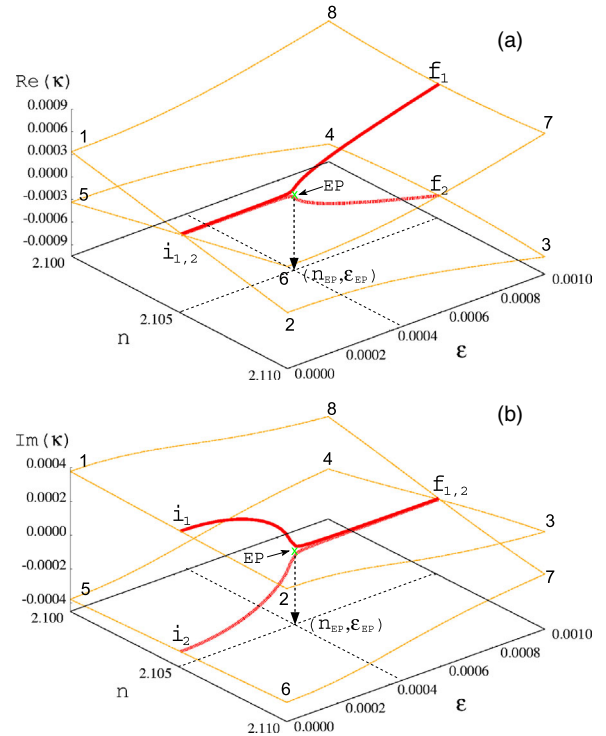

FIG. 2. Degree of degeneracy of mode pairs (l, m) and $(l + 1, m - 4)$ given by Eq. (3) as a function of m and n at $\varepsilon = 0$.

FIG. 3. Real (a) and imaginary (b) part of the shifted frequency κ as a function of n and ε calculated with the BEM. The labels i_1 and i_2 correspond to the modes $(l, m) = (1, 22)$ and $(2, 18)$, respectively; cf., Fig. 2. The EP is at $(n_{\text{EP}}, \varepsilon_{\text{EP}}) \approx (2.1051, 0.000\,434)$.
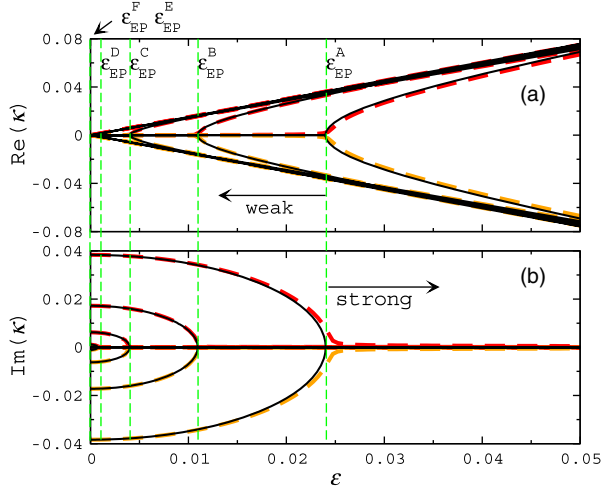
FIG. 4. Real (a) and imaginary (b) part of the shifted frequency κ as a function of the deformation parameter ε for $l = 2$ modes. Thick-dashed curves and thin-solid curves are the results of the BEM and Eq. (7). Dashed vertical lines stand for $\varepsilon_{\mathrm{EP}}^{j}$ separating the weak and the strong coupling regime where the superscript j refers to $A, B, \ldots$ in Fig. 2. The deformation for E and F is too weak to be shown here ($\varepsilon_{\mathrm{EP}}^{E/F} < 10^{-5}$).

with $p_{t:r} = \cos(t\pi/r)$ and a global phase $\phi_0 = \pi$. The amplitude $\mathcal{V}_{t:r}$ in the Hamiltonian (4) can be expressed in terms of the trace of monodromy matrix $M_{t:r}$ of the stable periodic ray in the center of the resonance chain [21],

$$\mathcal{V}_{t:r}(\varepsilon) = \frac{L(\varepsilon)^2\sqrt{1 - p_{t:r}^2}}{16\pi^2 r^4}\left[\arccos\left(\frac{\mathrm{Tr}M_{t:r}(\varepsilon)}{2}\right)\right]^2. \quad (5)$$

We find that this coupling strength $\mathcal{V}_{t:r}$ can be used in the exact Hamiltonian in the basis of the unperturbed solutions of Eq. (2) with a scaling constant

$$V(\varepsilon) = \gamma_{t:r}\mathcal{V}_{t:r}(\varepsilon), \quad (6)$$

where $\gamma_{t:r} = \mathrm{Re}(n_{\mathrm{EP}}k_0R)(2\sqrt{1 - p_{t:r}^2})^{-1}$ is obtained empirically and is confirmed numerically for several $(1{:}r)$-resonance chains with $r = 3, 4, 5$ and different values of n_{EP}. Here, k_0 is a solution of Eq. (2) at $n = n_{\mathrm{EP}}$. Accordingly, the Hamiltonian reads

$$H = \begin{pmatrix} \kappa_{l,m}(n_{\mathrm{EP}}, \varepsilon) & \gamma_{t:r}\mathcal{V}_{t:r}(\varepsilon) \\ \gamma_{t:r}\mathcal{V}_{t:r}(\varepsilon) & \kappa_{l+t,m-r}(n_{\mathrm{EP}}, \varepsilon) \end{pmatrix}. \quad (7)$$

For the $(t{:}r) = (1{:}4)$-resonance chain, the eigenvalues of H, corresponding to the modes $A, B, \ldots$ of $l = 2$ in Fig. 2, are shown in Fig. 4 in perfect agreement with the BEM results. The diagonal elements in H depend on ε, following the area variation of the cavity [26]. However, since the modes (l, m) and $(l + 1, m - 4)$ are here influenced by almost the same amount, we can neglect the ε dependency, $\kappa(n_{\mathrm{EP}}, \varepsilon) \approx \kappa(n_{\mathrm{EP}}, 0)$.

Using the Hamiltonian (7) the condition for the EP is then

$$\gamma_{1:4}\mathcal{V}_{1:4}(\varepsilon) = \pm\frac{i}{2}[\kappa_{l,m}(n_{\mathrm{EP}}, 0) - \kappa_{l+1,m-4}(n_{\mathrm{EP}}, 0)]. \quad (8)$$

The rhs is real since n has been fine-tuned such that $\mathrm{Re}[\kappa_{l,m}(n_{\mathrm{EP}}, 0)] = \mathrm{Re}[\kappa_{l+1,m-4}(n_{\mathrm{EP}}, 0)]$. This implies that condition (8) can be fulfilled by varying ε alone, explaining $n \approx \mathrm{const}$ along the path to the EP in Fig. 3.

Figure 5 compares the real-space intensity of the modes [corresponding to the eigenstates of H in Eq. (7)] near the EP to their phase-space projections in terms of the Husimi functions [30]. Whereas modes 1, 2, 5, and 6 are conventional whispering gallery modes, modes 3, 4, 7, and 8 exhibit a localization along the periodic rays due to interference [31]. As expected, the Husimi functions show that this is in reasonable approximation related to the stable (7, 8) and unstable (3, 4) periodic ray in the $(1{:}4)$-resonance chain.

Figure 6 shows the modes involved in the transition through the EP. Interestingly, at the EP an abnormal localization can be observed. The mode is neither localized on the stable periodic ray trajectory nor on the unstable one but in between them. The abnormal localization disappears for $\varepsilon \gg \varepsilon_{\mathrm{EP}}$ (not shown). In order to reveal the origin of the abnormal localization we mention that the single eigenvector at a second-order EP is [33]

$$|\Psi\rangle_{\mathrm{EP}} \propto (1, \pm i)^T \quad (9)$$

in a basis of standing waves, with either $+$ or $-$. The superposition of the modes corresponding to this eigenvector $\Psi_{\pm i} \sim \psi_1^0 \pm i\psi_2^0$ possesses chirality [33]. In our situation, it turns out that they have a vortex structure
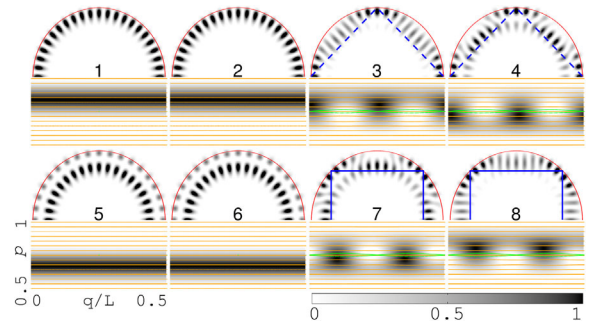

FIG. 5. Intensity and incident Husimi function of the modes marked by the same labels as in Fig. 3. The maximum value is normalized to be unity. The labels 1, 2, 5, and 6 mark whispering gallery modes whereas modes 3, 4, 7, and 8 exhibit localization around the period-4 rays (solid, stable; dashed, unstable). The superimposed resonance chain in 3, 4, 7, and 8 is vertically shifted according to the periodic ray shift due to the Goos-Hänchen shift [32].
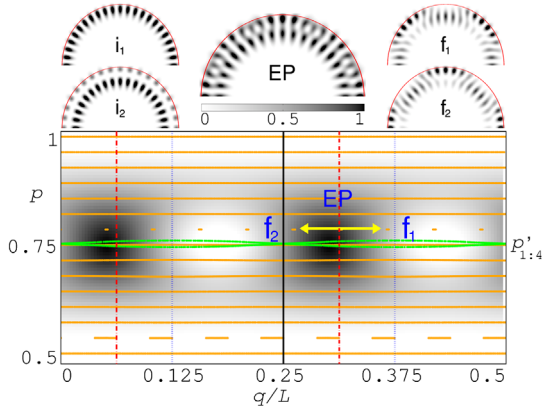
FIG. 6. Intensity and incident Husimi function of the modes marked by the same labels as in Fig. 3. The Husimi function is the one at the EP. $p'_{1:4}$ is a vertically shifted (1:4)-resonance chain as in Fig. 5. The arrows indicate the direction of the Husimi function movement of the two modes when $\varepsilon > \varepsilon_{EP}$ after the bifurcation of $\mathrm{Re}(\kappa)$. The maximum value is normalized to be unity.

[see Fig. 7(c)] that induces a local spatial chirality of the wave propagation.

The local chirality, i.e., the alternating wave propagation direction along the cavity boundary first observed in a strongly deformed cavity with chaotic ray dynamics [34], causes here the abnormal localization of the Husimi function in Fig. 6. At the EP, the Husimi function and the vortices are explained by the superpositions of the circular cavity's modes according to Eq. (9). In Fig. 8, the Poynting vector of Ψ_{-i} of the lower half boundary shows the counterclockwise ($p > 0$) propagation direction whereas the upper part shows the clockwise ($p < 0$) propagation direction. Thus, the Husimi function around $q/L = 1/16 = 0.0625$ is on the upper half of phase space
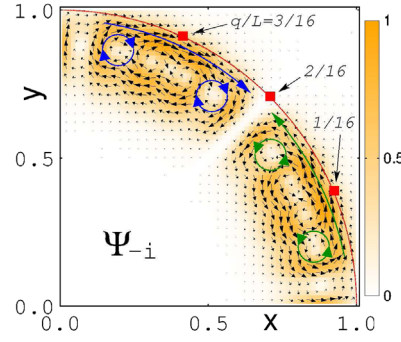

FIG. 8. Superposition $\Psi_{-i} = \psi^c_{1,22} - i\psi^c_{2,18}$ and corresponding $\vec{J}$ where $\psi^c_{l,m}$ is a mode in the circular cavity; cf., Fig. 7(c). Shading represents $|\vec{J}|$ normalized to be unity at maximum.

while $q/L = 3/16 = 0.1875$ is on the lower half of phase space, which is fully consistent with Fig. 6.

Figures 7(a) and 7(b) reveal that the EPs of EE and OO modes are nearly degenerated, which is consistent with the fact that RAT does here not depend on the parity. The vortex structure [Figs. 7(c) and 7(d)] and the Husimi functions (EE in Fig. 6, and OO not shown) are also almost the same. The near degeneracy of the EPs is important because a fourth-order EP can be possibly constructed by an additional weak deformation that couples the two symmetry classes by breaking the mirror-reflection symmetry of the cavity. A fourth-order EP is expected to generate even higher sensitivity than second-order EPs in sensor applications [35].

For a demonstration of the general validity of our arguments, we apply Eq. (7) to another system and confirm a nearly perfect agreement with full numerics. One example of a $(t:r) = (1:3)$-resonance chain in the cavity

$$\rho(\theta) = R[1 + \varepsilon \cos(3\theta)] \tag{10}$$

is given in Fig. 9. Here, the even- and odd-parity modes are almost identical; thus, only the even mode is displayed in Fig. 9.
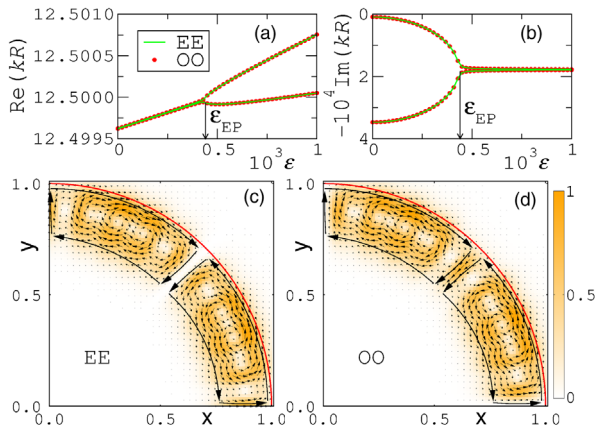

FIG. 7. Real (a) and imaginary (b) part of the frequency of $(l, m) = (1, 22)$ and $(2, 18)$ modes with EE and OO parity computed by the BEM. Poynting vector $\vec{J} \equiv \mathrm{Im}(\psi^* \vec{\nabla} \psi)$ of the mode at the EP for EE (c) and OO (d). Long arrows in (c) and (d) illustrate the average flow. Shading represents $|\vec{J}|$ normalized to be unity at the maximum value.
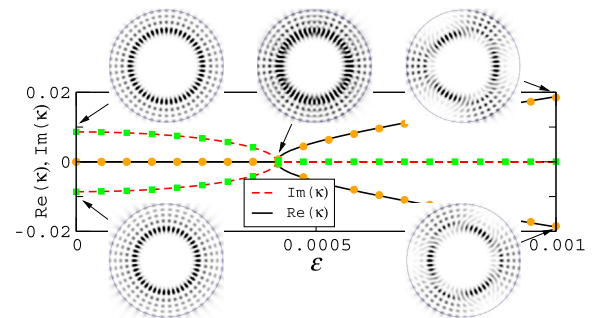

FIG. 9. Complex frequencies of the modes $(l, m) = (5, 21)$ and $(4, 24)$, satisfying a Fermi resonance condition $(\Delta l, \Delta m) = (1, 3)$, for the cavity in Eq. (10) as a function of the deformation parameter ε. The EP is at $(n_{EP}, \varepsilon_{EP}) = (2.3388, 0.000 \, 421 \, 3)$. Solid squares and circles are obtained from the BEM and solid and dashed curves are given by Eq. (7) for a $(t:r) = (1:3)$-resonance chain.

To summarize, we demonstrated the appearance of exceptional points in extremely weakly deformed microcavities. The finding is explained and motivated by resonance-assisted tunneling. Extremely weak deformation promises the ultranarrow linewidth of modes on exceptional points, which will boost up the order of sensitivity in sensor applications. No fragile external perturbations such as by nanofiber tips (see Ref. [25]) are needed to implement the exceptional point. This fact is clearly advantageous for applications. We have shown that the abnormal localization of Husimi functions at the exceptional point is originated from local vortices of the Poynting vector, which induces a spatially local chirality. Nearly degenerated exceptional points of different symmetry classes were observed. This finding is also significant since it implies the possibility of fourth-order exceptional points, which provides an additional enhancement of sensitivity.

*changhwan.yi@ovgu.de

[1] T. Kato, *Perturbation Theory for Linear Operators* (Springer, New York, 1966); W. D. Heiss, Phys. Rev. E **61**, 929 (2000); M. V. Berry, Czech. J. Phys. **54**, 1039 (2004).

[2] C. E. Rüter, K. G. Makris, R. El-Ganainy, D. N. Christodoulides, M. Segev, and D. Kip, Nat. Phys. **6**, 192 (2010); C. Shi, M. Dubois, Y. Chen, L. Cheng, H. Ramezani, Y. Wang, and X. Zhang, Nat. Commun. **7**, 11110 (2016).

[3] Y. Ashida, S. Furukawa, and M. Ueda, Nat. Commun. **8**, 15791 (2017); B.-B. Wei and L. Jin, Sci. Rep. **7**, 7165 (2017).

[4] H. Cartarius, J. Main, and G. Wunner, Phys. Rev. Lett. **99**, 173003 (2007).

[5] B. Alfassi, O. Peleg, N. Moiseyev, and M. Segev, Phys. Rev. Lett. **106**, 073901 (2011).

[6] M. Liertzer, L. Ge, A. Cerjan, A. D. Stone, H. E. Türeci, and S. Rotter, Phys. Rev. Lett. **108**, 173901 (2012).

[7] C. Dembowski, H.-D. Gräf, H. L. Harney, A. Heine, W. D. Heiss, H. Rehfeld, and A. Richter, Phys. Rev. Lett. **86**, 787 (2001); J. Doppler, A. A. Mailybaev, J. Böhm, U. Kuhl, A. Girschik, F. Libisch, T. J. Milburn, P. Rabl, N. Moiseyev, and S. Rotter, Nature (London) **537**, 76 (2016).

[8] B. Peng, Ş. K. Özdemir, M. Liertzer, W. Chen, J. Kramer, H. Yilmaz, J. Wiersig, S. Rotter, and L. Yang, Proc. Natl. Acad. Sci. U.S.A. **113**, 6845 (2016); M. Brandstetter, M. Liertzer, C. Deutsch, P. Klang, J. Schöberl, H. E. Türeci, G. Strasser, K. Unterrainer, and S. Rotter, Nat. Commun. **5**, 4034 (2014).

[9] H.-J. Stöckmann, *Quantum Chaos* (Cambridge University Press, Cambridge, 2000).

[10] M. J. Davis and E. J. Heller, J. Chem. Phys. **75**, 246 (1981); S. D. Frischat and E. Doron, Phys. Rev. E **57**, 1421 (1998).

[11] S. Keshavamurthy and P. Schlagheck, *Dynamical Tunneling: Theory and Experiment* (Taylor & Francis, 2011);

N. Mertig, J. Kullig, C. Löbner, A. Bäcker, and R. Ketzmerick, Phys. Rev. E **94**, 062220 (2016); C.-H. Yi, H.-H. Yu, and C.-M. Kim, Phys. Rev. E **93**, 012201 (2016).

[12] A. J. Lichtenberg and M. A. Lieberman, *Regular and Chaotic Dynamics* (Springer, Berlin, 1992).

[13] O. Brodier, P. Schlagheck, and D. Ullmo, Phys. Rev. Lett. **87**, 064101 (2001); S. Löck, A. Bäcker, R. Ketzmerick, and P. Schlagheck, Phys. Rev. Lett. **104**, 114101 (2010); F. Fritzsch, A. Bäcker, R. Ketzmerick, and N. Mertig, Phys. Rev. E **95**, 020202 (2017).

[14] A. M. Ozorio de Almeida, J. Phys. Chem. **88**, 6139 (1984).

[15] A. Ramamoorthy, R. Akis, J. P. Bird, T. Maemoto, D. K. Ferry, and M. Inoue, Phys. Rev. E **68**, 026221 (2003).

[16] S. Shinohara, T. Harayama, T. Fukushima, M. Hentschel, T. Sasaki, and E. E. Narimanov, Phys. Rev. Lett. **104**, 163902 (2010); Q. H. Song, L. Ge, B. Redding, and H. Cao, Phys. Rev. Lett. **108**, 243902 (2012).

[17] C. Dembowski, H.-D. Gräf, A. Heine, R. Hofferbert, H. Rehfeld, and A. Richter, Phys. Rev. Lett. **84**, 867 (2000); A. Bäcker, R. Ketzmerick, S. Löck, M. Robnik, G. Vidmar, R. Höhmann, U. Kuhl, and H.-J. Stöckmann, Phys. Rev. Lett. **100**, 174103 (2008).

[18] W. K. Hensinger, H. Haffner, A. Browaeys, N. R. Heckenberg, K. Helmerson, C. McKenzie, G. J. Milburn, W. D. Phillips, S. L. Rolston, H. Rubinsztein-Dunlop, and B. Upcroft, Nature (London) **412**, 52 (2001).

[19] H. Cao and J. Wiersig, Rev. Mod. Phys. **87**, 61 (2015); X. Jiang, L. Shao, S.-X. Zhang, X. Yi, J. Wiersig, L. Wang, Q. Gong, M. Lončar, L. Yang, and Y.-F. Xiao, Science **358**, 344 (2017).

[20] J. Wiersig, S. W. Kim, and M. Hentschel, Phys. Rev. A **78**, 053809 (2008); J.-W. Ryu and S.-Y. Lee, Phys. Rev. E **83**, 015203(R) (2011); J. Wiersig, A. Eberspächer, J.-B. Shim, J.-W. Ryu, S. Shinohara, M. Hentschel, and H. Schomerus, Phys. Rev. A **84**, 023845 (2011); S.-B. Lee, J. Yang, S. Moon, S.-Y. Lee, J.-B. Shim, S. W. Kim, J.-H. Lee, and K. An, Phys. Rev. Lett. **103**, 134101 (2009).

[21] J. Kullig and J. Wiersig, Phys. Rev. E **94**, 022202 (2016).

[22] C.-H. Yi, J. Kullig, C.-M. Kim, and J. Wiersig, Phys. Rev. A **96**, 023848 (2017).

[23] H. Kwak, Y. Shin, S. Moon, S.-B. Lee, J. Yang, and K. An, Sci. Rep. **5**, 9010 (2015).

[24] J. Wiersig, Phys. Rev. Lett. **112**, 203901 (2014); J. Kullig and J. Wiersig, Phys. Rev. A **94**, 043850 (2016).

[25] W. Chen, Ş. Kaya Özdemir, G. Zhao, J. Wiersig, and L. Yang, Nature (London) **548**, 192 (2017).

[26] R. Dubertrand, E. Bogomolny, N. Djellali, M. Lebental, and C. Schmit, Phys. Rev. A **77**, 013804 (2008).

[27] C.-H. Yi, H.-H. Yu, J.-W. Lee, and C.-M. Kim, Phys. Rev. E **91**, 042903 (2015).

[28] J. Wiersig, J. Opt. A **5**, 53 (2003).

[29] J. Kullig, C. Löbner, N. Mertig, A. Bäcker, and R. Ketzmerick, Phys. Rev. E **90**, 052906 (2014).

[30] M. Hentschel, H. Schomerus, and R. Schubert, Europhys. Lett. **62**, 636 (2003).

[31] J. Unterhinninghofen, J. Wiersig, and M. Hentschel, Phys. Rev. E **78**, 016201 (2008).

[32] J. Unterhinninghofen and J. Wiersig, Phys. Rev. E **82,** 026202 (2010).

[33] W. D. Heiss and H. L. Harney, Eur. Phys. J. D **17,** 149 (2001); C. Dembowski, B. Dietz, H.-D. Gräf, H. L. Harney, A. Heine, W. D. Heiss, and A. Richter, Phys. Rev. Lett. **90,** 034101 (2003).

[34] B. Redding, L. Ge, Q. H. Song, J. Wiersig, G. S. Solomon, and H. Cao, Phys. Rev. Lett. **108,** 253902 (2012).

[35] H. Hodaei, A. U. Hassan, S. Wittek, H. Garcia-Gracia, R. El-Ganainy, D. N. Christodoulides, and M. Khajavikhan, Nature (London) **548,** 187 (2017).